

C 4 Elasticity, Friction and Fracture

R. Spatschek

Institut für Festkörperforschung

Forschungszentrum Jülich GmbH

Contents

1	Introduction	2
2	Linear Elasticity	2
2.1	Plane strain	4
3	Applications	5
3.1	Fracture	5
3.2	Adhesion and Friction	7
3.3	Dislocations	11
3.4	Earthquakes	12
4	Numerical Methods	13
4.1	Classification of partial differential equations	13
4.2	Finite difference methods	14
4.3	Finite Element Method (FEM)	17
4.4	Boundary Element Method (BEM)	21
4.5	Discussion	25
A	The static semi-infinite crack	26

1 Introduction

It is hard to imagine our world without the various manifestations of elastic effects. Fracture, for example, is an intriguing irreversible phenomenon that plays an important role in our day-to-day-life. Cracks occur on all scales from nano- to kilometers: we observe them in geological formations and earthquakes, semiconductor-metal-contacts, airplane wings and buildings. They are responsible for the vast field of material failure and also for friction processes: slip motion between different solids can be interpreted as a traveling of self-healing cracks along the contact area of the interface. Complicated patterns of crack networks appear in drying mud. Every day, engineers perform elastic calculations to design buildings and cars.

During the past decades, numerical methods have become extremely important in solving the underlying partial differential equations. Therefore, it is the aim of this article to present both the fundamental physical effects and suitable numerical techniques to model them.

Unfortunately, we can discuss here only a few aspects of these fascinating phenomena. In particular, we restrict ourself to the linear theory of elasticity, though especially in fracture stresses can become large that such a theory fails and plastic or viscoelastic effects come into the play. Also, we mainly discuss static elasticity, though many ideas can be directly translated to dynamical theories which account for the whole spectrum of wave propagation.

2 Linear Elasticity

We assume that all quantities are given in a fixed, orthonormal frame of reference. The coordinates of all points of the undisplaced body are given by a vector field x_i . External forces deform the body, and the mass points move to new coordinates $x_i^*(\{x_j\})$, which are functions of the original coordinates. The quantity

$$u_i(\{x_j\}) = x_i^*(\{x_j\}) - x_i \quad (1)$$

is called *displacement vector* and is assumed to be small. The *strain field* is defined as

$$\epsilon_{ij} = \frac{1}{2} \left(\frac{\partial u_i}{\partial x_j} + \frac{\partial u_j}{\partial x_i} \right), \quad (2)$$

which is a symmetric tensor.

The *stress field* is denoted by σ_{ij} . Its physical meaning is that its component i gives the elastic force density per unit area which acts on a plane with normal vector in j direction. The conservation of angular momentum implies the symmetry of σ_{ij} [1]. In the linear theory of elasticity the connection between stresses and strain is given by *Hooke's law*; in the special case of isotropic materials it becomes:

$$\sigma_{ij} = \frac{E}{1 + \nu} \left(\epsilon_{ij} + \frac{\nu}{1 - 2\nu} \delta_{ij} \epsilon_{kk} \right), \quad (3)$$

with E being the elastic modulus and ν the Poisson ratio. The first one is a measure for the strength of a material and has the dimension of a pressure. For steel, it is $E \approx 200\text{GPa}$. The Poisson ratio is a dimensionless number in the range $0 < \nu < 1/2$ and expresses how much an elastic body shrinks in a direction perpendicular to an applied pulling force. Alternatively, the constitutive relation (3) can be expressed in terms of the shear modulus $\mu = E/[2(1 + \nu)]$ and

the Lamé coefficient $\lambda = \nu E / [(1 + \nu)(1 - 2\nu)]$. In Eq. (3) we make use of the sum convention, which means that we sum over all indices which appear twice in an expression. Specifically, it contains a sum $\sum_{k=1}^3$ which is not written explicitly.

More generally, stress and strain are related by $\sigma_{ij} = c_{ijkl}\epsilon_{kl}$, but we confine ourself to the isotropic case here. Also, we do not take thermal expansion into account.

The inverse transformation to Eq. (3) is

$$\epsilon_{ij} = \frac{1}{E} [(1 + \nu)\sigma_{ij} - \nu\delta_{ij}\sigma_{kk}]. \quad (4)$$

The time evolution of the mechanical state is described by Newton's equation of motion, which reads

$$\frac{\partial \sigma_{ij}}{\partial x_j} + f_i = \rho \ddot{u}_i, \quad (5)$$

with a density f_i of volume forces and the mass density ρ . A typical example for volume forces is gravitation, but nevertheless we assume $f_i = 0$ for our further analysis. In many cases, the right hand side can be neglected (static elasticity). The term $\partial \sigma_{ij} / \partial x_j$ is the density of elastic forces acting on each mass element. It can easily be understood by considering a small cube of material with volume dx^3 and by evaluating the elastic forces on all six fronts. For example, the forces on the two opposite fronts at $x = 0$ and $x = dx$ are $-dx^2 \sigma_{xx}(x = 0)$ and $dx^2 \sigma_{xx}(x = dx)$ respectively. Therefore, the sum of them is $dx^3 \partial \sigma_{xx} / \partial x$, and similar contributions arise from the other fronts of the cube.

Quite often one discusses elastic problems on the level of strains and stresses instead of displacements. However, it has to be assured that they can be derived from the latter ones. The necessary integrability condition is called *St. Venant's compatibility condition*:

$$\frac{\partial^2 \epsilon_{ij}}{\partial x_k \partial x_l} + \frac{\partial^2 \epsilon_{kl}}{\partial x_i \partial x_j} = \frac{\partial^2 \epsilon_{ik}}{\partial x_j \partial x_l} + \frac{\partial^2 \epsilon_{jl}}{\partial x_i \partial x_k}. \quad (6)$$

Solving an elastic problem requires apart from satisfaction of the bulk equations (5) the fulfillment of boundary conditions, which can be either conditions for the displacement or the stresses. The first case is important if the elastic body is attached to a rigid handle such that the atoms at the boundary can not move freely. In the second case, forces are applied at the boundary. However, not all stress components can be accessed at the boundary: Assume for simplicity that the boundary is located at the plane $x = 0$. Then only σ_{xx} , $\sigma_{xy} = \sigma_{yx}$ and $\sigma_{xz} = \sigma_{zx}$ can be set, since they determine the force which is acting on the specific plane. In particular, the latter two stresses correspond to shear forces. The other components, σ_{yy} , σ_{zz} and σ_{yz} , cannot be fixed as boundary conditions but are determined through the solution of the problem.

In more general cases, the interface is not necessarily perpendicular to the coordinate axes, and therefore the stress tensor has to be expressed in a different coordinate system. Let $n = (n_1, n_2, n_3)$ and $\tau = (\tau_1, \tau_2, \tau_3)$ be the coordinates of two normalized vectors in x, y, z representation. Then the stress component $\sigma_{n\tau}$, i. e. the τ component of the force density acting on a plane with normal n (or vice versa), is given by

$$\sigma_{n\tau} = n_i \sigma_{ij} \tau_j, \quad (7)$$

where we used again the sum convention.

The potential and kinetic energy which is stored in a deformed body Ω is given by

$$U + T = \int_{\Omega} \left(\frac{1}{2} \sigma_{ij} \epsilon_{ij} + \frac{1}{2} \rho \dot{u}_i^2 \right) d\Omega. \quad (8)$$

Its rate of change is related to the work of the external forces (acting only at the boundary),

$$\frac{d(U + T)}{dt} = \int_{\Gamma} \sigma_{in} \dot{u}_i d\Gamma, \quad (9)$$

which follows directly from the equation of motion (5) and Gauss' theorem.

Whenever processes become fast, dynamical effects can become relevant in the theory of elasticity, which happens e. g. in fast crack propagation. The characteristic velocity scale is the speed of sound $c \sim (E/\rho)^{1/2}$, which ranges from a few meters per second in gels to thousands of meters per second in rigid materials. For isotropic elasticity, the propagation velocities for longitudinal and shear waves, c_d and c_s respectively, can easily be calculated to be

$$c_d = \left(\frac{E(1-\nu)}{\rho(1-2\nu)(1+\nu)} \right)^{1/2}, \quad c_s = \left(\frac{E}{2\rho(1+\nu)} \right)^{1/2}. \quad (10)$$

In seismology, these velocities are usually called *P-wave* (primary wave) and *S-wave* (secondary wave), as the dilatational sound speed is higher and therefore these waves are recorded earlier. *Rayleigh* and *Love* waves are surface waves and are also recorded in seismic measurements.

2.1 Plane strain

Two-dimensional situations are very important for many applications. Special techniques can be used to solve the elastic equations, among them the conformal mapping method which will not be explained here [2]. The basic idea is that the elastic fields can be represented by analytical complex functions. Solutions for simple geometries like a spherical hole in an infinite medium can easily be determined analytically. If a conformal mapping can be found which maps a more complicated problem to a simpler situation, then the inverse transformation can be used to solve the real problem.

Two different types of two-dimensional limits of the elastic equations are important in practice. The first one is the *plane stress* scenario which is relevant for example for thin layers. Since by boundary conditions the normal and shear stresses have to vanish on both sides of the film, the approximation that they vanish also inside the sheet is reasonable. Displacements, however, can be out-of plane.

The other case is called *plane strain*, which is relevant for in-plane distortions in thick samples. Since both situations can be mapped to each other, we discuss only the latter one here. Here, all displacements are within the xy plane, i. e. $u_z = 0$. Furthermore, u_x and u_y depend only on x and y , thus

$$\sigma_{xz} = \sigma_{zx} = \sigma_{yz} = \sigma_{zy} = 0 \quad (11)$$

and

$$\sigma_{zz} = \frac{\nu E}{(1+\nu)(1-2\nu)}. \quad (12)$$

A simple technique to solve the static elastic problem is the use of the *Airy function* $\chi(x, y)$. We assume that the stresses are derived from this function by virtue of

$$\sigma_{xx} = \frac{\partial^2 \chi}{\partial y^2}, \quad \sigma_{xy} = -\frac{\partial^2 \chi}{\partial x \partial y}, \quad \sigma_{yy} = \frac{\partial^2 \chi}{\partial x^2}. \quad (13)$$

If we can find a proper function $\chi(x, y)$, then the bulk equations $\partial_i \sigma_{ik} = 0$ (without bulk forces) are automatically satisfied. Then we can easily calculate the strain field using Hooke's law, but

we have to assure that this field can be derived from a displacement field. The integrability condition (6) reduces to the *biharmonic equation*

$$\nabla^4 \chi = 0 \quad \text{or} \quad \frac{\partial^4 \chi}{\partial x^4} + 2 \frac{\partial^4 \chi}{\partial x^2 \partial y^2} + \frac{\partial^4 \chi}{\partial y^4} = 0. \quad (14)$$

A simple illustration is a homogeneously stretched body; here, a tensile or compressive stress P is applied in x -direction. A proper Airy function is $\chi = \frac{1}{2}Py^2$, from which we obtain the stresses $\sigma_{xx} = P, \sigma_{xy} = \sigma_{yy} = 0$. Obviously, the biharmonic equation is fulfilled, which means that indeed a valid displacement state exists. The strain field is $\epsilon_{xx} = P(1 - \nu^2)/E$, $\epsilon_{yy} = -\nu(1 + \nu)P/E$ and $\epsilon_{xy} = 0$. It can easily be integrated using the definition of the strain tensor (2), and we obtain $u_x = x(1 - \nu^2)P/E$ and $u_y = -y\nu(1 + \nu)P/E$. Integration constants corresponding to a translational motion and a rigid body rotation are not interesting and are therefore suppressed. We also want to mention that from this results the meaning of the Poisson ratio becomes obvious: with $\nu = 0$ the sample does not shrink vertically if it is horizontally stretched.

3 Applications

3.1 Fracture

The fundamental idea about the energetic situation during crack formation was developed by Griffith in 1921 [3]. Consider an infinite two-dimensional solid which is subjected to an external tension P (see Fig. 1). For simplicity, the material is assumed to be homogeneous and isotropic,

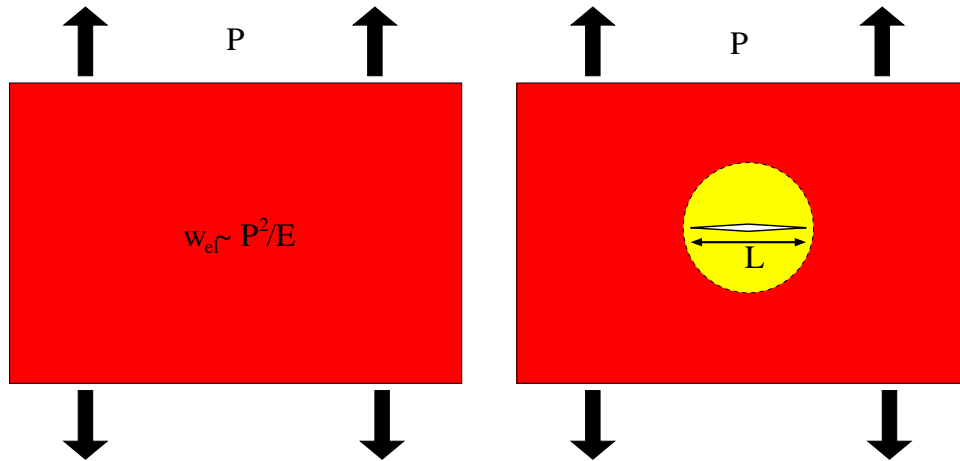


Fig. 1: An initially homogeneously stretched body reduces its elastic energy by producing a crack. On the other hand, this increases the surface energy of the system.

and the static linear theory of elasticity is used; dynamical effects become only relevant for fast fracture and are irrelevant for “crack nucleation processes”. In this homogeneously stressed solid, the elastic energy density is $w_{el} \sim P^2/E$, where E is the elastic modulus (we suppress the dimensionless Poisson ratio of order unity here, which does not alter the scaling behavior). We compare this situation to a solid which contains a finite crack of length L . Approximately, in the area $A \sim L^2$ the initial stress has relaxed by the opening of the crack. Therefore, we have

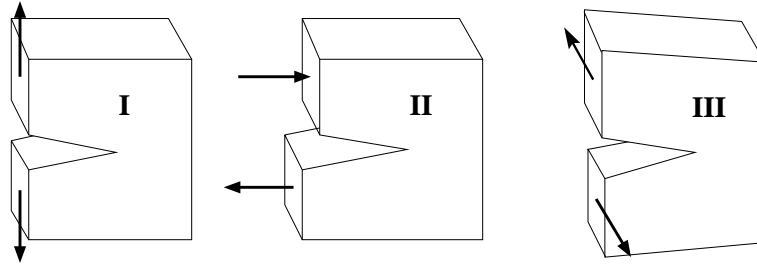


Fig. 2: The three different types of loading near a crack tip.

a decrease of the initially stored elastic energy by $W_{el} \sim w_{el}A \sim P^2L^2/E$ (per unit width of the sample). On the other hand, two new surfaces have been created which lead to a surface energy contribution $W_s \sim \gamma L$ with the surface energy density γ . The change of the total energy $W_{el} + W_s$ with respect to the situation without crack depends thus on the length of the crack: for short cracks the energy increases with the crack length L , but for sufficiently long cracks it is reduced, finally leading to complete rupture. The characteristic length scale

$$L_G \sim \frac{E\gamma}{P^2} \quad (15)$$

is called the *Griffith length* and determines whether a crack grows or shrinks (if a healing process is not hampered e. g. by oxidation).

So far, γ describes the energy to create surfaces, but it might contain other contributions as well. In particular, the strength of adhesion and cohesion can be characterized by the amount of energy γ to advance the crack. Notice that γ does not only include the energy to break the bonds at the crack tip, but also all the energy which is dissipated in the vicinity of the crack tip during crack propagation. For example, for rubber-like materials this also includes the viscoelastic energy dissipation which may occur several micrometers away from the crack tip. Therefore, it is not surprising that γ depends strongly on the propagation velocity and temperature. At extremely low velocities and high temperatures, when viscous effects e. g. in rubber are minimized, the surface energy density is of order $\gamma \sim 50\text{J/m}^2$. However, for high crack speeds, it may be up to 10^4 times higher.

In the vicinity of a crack tip stresses become large, and for a sharp tip they can even diverge like $\sigma \sim r^{-1/2}$ with r being the distance from the tip. We distinguish between three types of loading, the *opening mode* (mode I), *in-plane sliding* (mode II) and *anti-plane sliding* (mode III) (see Fig. 2). A general loading can always be decomposed into these three modes. In each case, stresses behave like

$$\sigma_{ij} = \frac{K}{(2\pi r)^{1/2}} f_{ij}(\theta). \quad (16)$$

The angular dependence $f_{ij}(\theta)$ is a universal dimensionless function for each loading mode (the polar angle θ is zero ahead of the crack tip). The scalar quantity K is called *stress intensity factor* and combines all the macroscopic properties of the crack including length, external forces and shape of the crack. With the characteristic external stress P and crack length L , the stress intensity factor behaves like

$$K \sim PL^{1/2}. \quad (17)$$

For mode I one gets explicitly

$$\begin{Bmatrix} \sigma_{xx} \\ \sigma_{xy} \\ \sigma_{yy} \end{Bmatrix} = \frac{K_I}{(2\pi r)^{1/2}} \cos(\theta/2) \begin{Bmatrix} 1 - \sin(\theta/2) \sin(3\theta/2) \\ \sin(\theta/2) \cos(3\theta/2) \\ 1 + \sin(\theta/2) \sin(3\theta/2) \end{Bmatrix}. \quad (18)$$

This is the exact solution for the singular part the stress field for a semi-infinite crack (see appendix A for a derivation). Similar expressions can be found for running cracks,

$$\sigma_{ij} = K_{dyn}(v/c_R) \frac{f_{ij}(\theta, v/c_R)}{(2\pi r)^{1/2}}, \quad (19)$$

where both the angular distribution f_{ij} and the *dynamical stress intensity factor* K_{dyn} depend on the steady state propagation velocity v . Here, $c_R \sim (E/\rho)^{1/2}$ is the *Rayleigh speed*, which is the sound speed of waves traveling along a free surface, obeying $c_R < c_s < c_d$. In the limiting case $v \rightarrow 0$, the dynamical stress intensity factor matches the static one, $K_{dyn} \rightarrow K$, whereas for a long crack in a narrow strip $K_{dyn} \rightarrow 0$ if the crack speed approaches the Rayleigh speed. Therefore, in steady state, cracks cannot propagate faster than the the Rayleigh speed. In reality, however, the propagation velocity remains appreciably below c_R for many materials, as the cracks start to split and form complicated patterns.

In most materials, the stress singularity $\sigma \sim 1/r^{1/2}$ cannot be valid very close to the tip, but will yield. In an ideal brittle material, the above relations may hold until $r \sim a$ is of the order of a lattice constant a , but in most materials this relation breaks down at much larger distances. The spatial region where the relation $\sigma \sim 1/r^{1/2}$ is no longer valid is called the *crack tip process zone*.

Elongation of a crack reduces the elastic energy which is stored in the system. The rate of change is given by [4, 5]

$$-\frac{dU_{el}}{dL} = \frac{1 - \nu^2}{E} (K_I^2 + K_{II}^2) + \frac{1}{2\mu} K_{III}^2. \quad (20)$$

Then the Griffith point is determined by the equilibrium of elastic and surface energy

$$\frac{dU_{el}}{dL} + 2\gamma = 0. \quad (21)$$

3.2 Adhesion and Friction

Many aspects of adhesion involve crack propagation. The probably most fundamental adhesion problem is a spherical object on a flat surface (see Fig. 3 left). Both surfaces are assumed to be perfectly smooth and clean and at least one of them should be elastically soft. The contact area between the solids is circular and has radius r_0 . The radius of the sphere is denoted by R . The contact area is determined by the competition of the elastic energy and the change in surface energy, $\gamma = \gamma_1 + \gamma_2 - \gamma_{12}$. Here, γ_1, γ_2 are the surface energies (per unit area) of the phases with respect to the vacuum, γ_{12} is the interfacial energy between the two materials.

When an elastic ball is squeezed against a flat substrate, the pressure distribution acting on the contact area is given by [6]

$$P(r) = \frac{2E^*}{\pi R} (r_0^2 - r^2)^{1/2} - C(r_0^2 - r^2)^{-1/2}, \quad (22)$$

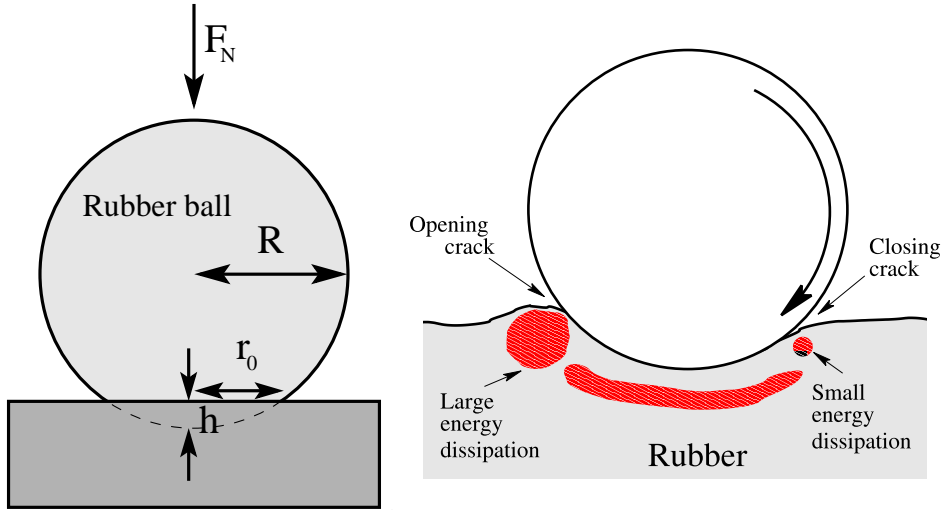


Fig. 3: Left: A rubber ball in contact with a hard flat substrate. The contact region is circular with radius r_0 . The radius of the ball is $R \gg r_0$, and the applied force F_N can be either positive (squeezing) or negative (pull-off). The sphere is compressed by the amount h . Right: A hard cylinder or ball rolling on a flat rubber track. Most of the energy is dissipated at the trailing edge.

where C is a so far unknown constant. In Eq. (22) the effective elastic modulus E^* is defined through the elastic constants of the two phases,

$$1/E^* = (1 - \nu_1^2)/E_1 + (1 - \nu_2^2)/E_2. \quad (23)$$

Close to the edge $r \approx r_0$, the last term in (22) has the same square root singularity as a crack,

$$P(r) \approx -C(2r_0)^{-1/2}(r_0 - r)^{-1/2}.$$

We can therefore identify the stress intensity factor $K = C(\pi/r_0)^{1/2}$. Assuming static equilibrium, we have in analogy to the former results $K^2/E^* \sim \gamma$, which allows to determine the unknown coefficient $C \sim (E^*\gamma r_0)^{1/2}$.

The total normal load can be obtained by integration,

$$F_N = \int_{r=0}^{r_0} r P(r) dr \sim \frac{E^* r_0^3}{R} - r_0^{3/2} (E^* \gamma)^{1/2}. \quad (24)$$

The pull-off force to lift the sphere from the ground can be obtained by minimizing the load F_N with respect to r_0 ,

$$F_{\text{pull-off}} \sim \gamma R. \quad (25)$$

Crack propagation is also involved in rolling of a cylinder (or a sphere) with smooth surfaces on a smooth substrate, see Fig. 3 right. The leading edge of the contact area can be interpreted as a closing crack, and another crack is created at the trailing edge.

When a rubber block is sliding on a hard rough substrate, rubber particles will continuously be removed from the block. This wear process involves two different steps, namely the nucleation of crack-like defects and propagation of the cracks resulting in the detachment of rubber particles. These particles are often very small, e. g. tire tread block wear on road surfaces produces micrometer-sized rubber particles.

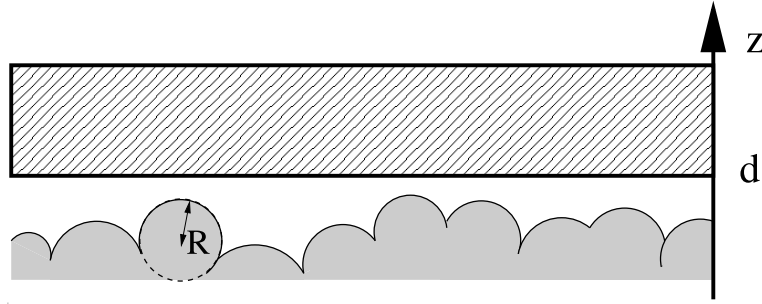


Fig. 4: Contact between a rough surface and a rigid plane.

Truck tires, where low rolling friction and high wear strength is more important than high tire-road friction, are usually produced from blends of butadiene rubber and natural rubber, while passenger car tires usually use mainly styrene-butadiene rubber in order to optimize the road-tire friction.

One of the most striking features of sliding friction is that the sliding force does not depend on the (macroscopic) contact area, as expressed through the well-known law,

$$F_S = \gamma_s F_N, \quad (26)$$

with the sliding friction coefficient γ_s . The explanation for this effect is that the *area of real contact* A_r is much smaller than the macroscopic contact area, since the two surfaces are microscopically rough and consist of many *asperities* (Fig. 4). This is also confirmed by experimental observations which show that A_r depends linearly on the applied normal force and that the frictional force increases linearly with A_r [7].

This observation seems to be paradoxical if we consider our previous results concerning the contact area of a single asperity under a normal load F_N : If we ignore the adhesive contribution, $\gamma = 0$ in Eq. (24), the area of real contact for a single asperity is

$$\pi r_0^2 \sim \left(\frac{F_N R}{E^*} \right)^{2/3}, \quad (27)$$

and therefore we would not expect the frictional force to increase linearly with the applied load, provided that all deformation is purely elastic, because the area of real contact obviously does not increase linearly with the normal force F_N . We also note that the sphere is compressed by

$$h \sim \frac{F_N}{E^* r_0} \sim \frac{F_N^{2/3}}{E^{*2/3} R^{1/3}}, \quad (28)$$

which follows from dimensional reasons.

The explanation of the paradox is related to the finite asperity height distribution, as can be seen from the following simple model calculation [8]. Let us approximate a surface as consisting of N elastic spherical caps with the same radius R but with different heights, which is pressed against a rigid flat plane (see Fig. 4). Let $N\Phi(z)dz$ be the number of spheres with heights between z and $z + dz$, i. e. $\Phi(z)$ is the height probability distribution. All asperities of height greater than d will make contact, and will be compressed a distance $h = z - d$. Therefore, according to Eqs. (27) and (28), the asperity contact area equals $\pi r_0^2 \sim \pi R h = \pi R(z - d)$ and

the asperity load equals $F_N \sim R^{1/2} h^{3/2} E^*$. Thus, the total number of contacts is

$$\Delta N = \int_d^\infty dz N \Phi(z),$$

the area of real contact

$$A_r^{(tot)} \sim \int_d^\infty dz N \Phi(z) \pi R (z - d),$$

and the total load

$$F_N^{(tot)} \sim \int_d^\infty dz N \Phi(z) R^{1/2} (z - d)^{3/2} E^*.$$

It is a reasonable (but not necessary) assumption that the rough surface has a Gaussian height distribution,

$$\Phi(z) = \left(\frac{1}{2\pi\ell^2} \right)^{1/2} e^{-(z-z_0)^2/2\ell^2},$$

where ℓ is proportional to the width of the distribution and z_0 is the average height of the rough surface. Close to $z = d$ the exponent can be expanded, so that

$$\Phi(z) \approx D e^{-\lambda(z-d)},$$

where

$$D = \left(\frac{1}{2\pi\ell^2} \right)^{1/2} e^{-(d-z_0)^2/2\ell^2}, \quad \lambda = \frac{d - z_0}{\ell^2}.$$

Using the above expression for $\Phi(z)$ leads to

$$\Delta N = ND/\lambda, \tag{29}$$

$$A_r^{(tot)} \sim NRD/\lambda^2, \tag{30}$$

$$F_N^{(tot)} \sim NR^{1/2} DE^* \lambda^{-5/2}. \tag{31}$$

Typically, the separation of the surfaces is $d \approx 2\ell - 3\ell$, therefore λ is rather constant in comparison to D , which depends exponentially on d . Hence, from Eq. (29), the normal force is almost proportional to the constant D , $F_N^{(tot)} \sim D$. Furthermore, from Eqs. (29)-(31), the number of contacts and the area of real contact is almost proportional to the normal load, in agreement with experiments and the observation (26). The origin of this result is that with increasing load $F_N^{(tot)}$, new contacts are continuously forming, initially with zero size and pressure, and the growth and formation exactly balance. A pure growth of the contact area with increasing load would not be proportional to the load if the number of contacts remains fixed, but since simultaneously new contacts are formed, the proportionality is re-established.

Apart from the microscopic roughness which leads to the effect that the area of real contact is much smaller than the macroscopic contact area, there can also be extended regions of detachment, see Fig. 5. For certain conditions of sliding between soft rubber and hard tracks, Schallamach has shown that the relative motion between the surfaces is due to waves of detachment crossing the contact zone. In some regions the two materials are “glued” to each other, and in between there are slip regions in which the surfaces move with some relative velocity against each other. The zones of detachment behave again like cracks, and the motion of the rubber block is due to the propagation of cracks between the solids.

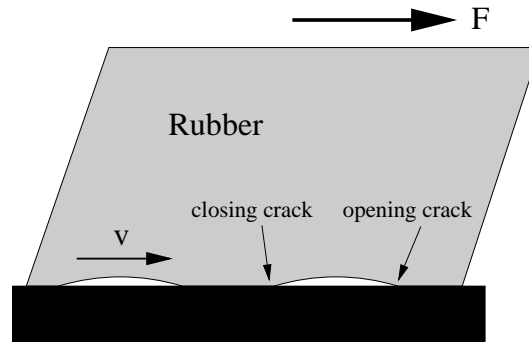


Fig. 5: Stick-slip motion of an elastic medium on a rigid substrate. “Cracks” propagate along the interface between the materials which leads to sound emission.

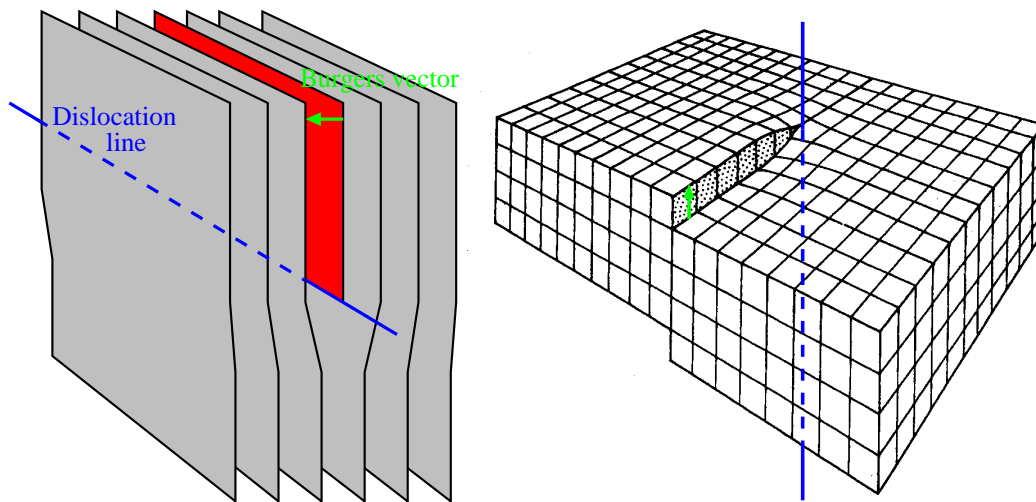


Fig. 6: Left: Sketch of an edge dislocation by insertion of an extra lattice plane (red). The dislocation line (blue) is located at the border of the lattice defect, the Burgers vector (green) measures the magnitude of the dislocation. Right: A screw dislocation.

3.3 Dislocations

In materials science, dislocations are defects or irregularities within a crystal structure. Whenever they appear, the compatibility conditions (6) are violated. The presence of dislocations strongly influences many of the properties of real materials, since they provoke elastic stresses. There are two major types of dislocations, *edge dislocations* and *screw dislocations*. Edge dislocations can be visualized as being formed by adding an extra half plane of atoms to a perfect crystal, so that a defect is created in the regular crystal structure along the line where the extra half-plane ends (Fig. 6 left).

The *dislocation line* surrounds the dislocation and is either a closed loop or must terminate at a boundary of the crystal. The *Burgers vector* characterizes the orientation and the magnitude of a dislocation, which is the width of the inserted plane for an edge dislocation. More formally, it is defined using a loop C enclosing the dislocation line. Then the Burgers vector is given by

the integral

$$b_i = \oint_C \frac{\partial u_i}{\partial l} dl, \quad (32)$$

with dl being a line element along C . For an edge dislocation, the dislocation line and the Burgers vector are perpendicular to each other. Notice that the integral above is zero everywhere in a defect-free crystal.

A screw dislocation is sketched in Fig. 6 (right). Here, the dislocation line and the Burgers vector are parallel to each other. The elastic displacement field of a straight screw dislocation can easily be guessed. We assume the dislocation line to be oriented in z direction and use polar coordinates r, φ in the xy plane with origin located at the dislocation line. There is no in-plane displacement, and obviously u_z is given by (b is the Burgers vector)

$$u_z = \frac{b\varphi}{2\pi}. \quad (33)$$

From this follows readily that stress and strain decay as $\epsilon \sim \sigma \sim 1/r$. Close to the dislocation line the strain becomes large and therefore the linear theory of elasticity breaks down in the *core region*. For an edge dislocation, the elastic fields are more complicated.

Usually, the dislocations present in real crystalline solids are rarely of a pure edge nature or pure screw, rather they exhibit aspects of both types, and are therefore termed *mixed dislocations*. Since the total energy of a system can depend on the separation of dislocations, there can be interacting forces between them. For further reading we recommend [9].

3.4 Earthquakes

Earthquakes generally result from a sudden rupture in the earth's crust, which occurs under the influence of slowly increasing compressive and shear tectonic stresses. Nucleation and propagation of such events take place along preexisting faults in the earth's crust. However, these weak paths are rarely planar but rather exhibit kinks, discontinuities, jogs, and varying levels of strength, which are of great importance in seismology. For example, branches and steps are believed to control the extend to which earthquake ruptures are able to propagate, thereby potentially restricting their magnitude [10].

The traditional engineering approach to fracture mechanics has been primarily guided by opening (mode I) cracks. As a crack in homogeneous, monolithic materials extends under the influence of external tractions, it will continually kink and assume a local mode I field, even if the external tractions are such as to generate mixed-mode stress states (*principle of local symmetry*). Seismologists, on the other hand, face different concerns. The earth's crust inherently contains numerous weak interfaces, or faults, and therefore from a fracture standpoint can no longer be construed as monolithic. In addition, active faulting brings rocks that are compositionally dissimilar into frictional contact, thereby inducing material inhomogeneity.

Consequently, earthquake ruptures are often modeled as dynamically propagating shear cracks with the aim of gaining insights into the physical mechanisms governing their arrest or, otherwise, the often observed variations in rupture speeds.

The moment magnitude scale (a successor to the Richter scale which defines the magnitude as the base-10 logarithm of the combined horizontal amplitude of the largest displacement from zero on a seismogram), was introduced in 1979 and is used by seismologists to compare the energy released by earthquakes. The moment magnitude M_w is a dimensionless quantity defined

by

$$M_w = \frac{2}{3} \left(\log_{10} \frac{M_0}{\text{Nm}} - 9.1 \right),$$

where M_0 is the seismic moment. It is defined by the equation $M_0 = \mu A u$, where μ is the shear modulus of the rocks involved in the earthquake, A is the area of the rupture along the geologic fault where the earthquake occurred, and u is the average displacement along the fault. An increase of 2 in the moment magnitude corresponds to a factor 1000 in the energy released during an earthquake.

Most large earthquakes are accompanied by other, smaller ones, that can occur either before or after the principal quake, known as *foreshocks* or *aftershocks*, respectively. Aftershocks are dangerous because they are usually unpredictable, can be of a large magnitude, and can collapse buildings that are damaged from the mainshock. The empirical Bath's law says that any mainshock typically has an aftershock on average 1.2 magnitude less than its mainshock. Also empirical is the Gutenberg-Richter scaling for aftershocks which states that the probability distribution for aftershocks of strength M_w is $P(M_w) \sim 10^{-bM_w}$ with a universal value $b \approx 1$. However, no satisfactory physical explanation for these laws has been found yet.

4 Numerical Methods

A huge variety of methods is available to solve elastic problems. Here, we discuss only the fundamental aspects of the three probably most important techniques:

- Finite Difference Methods
- Finite Element Methods
- Boundary Integral Methods

Since they are not restricted to elastic problems, we demonstrate them for the Laplace equation, the diffusion equation and the wave equation first. Afterwards, the application to elastic problems is elucidated. We restrict our considerations to simple linear, one- or two-dimensional problems, but it should be obvious how to generalize these approaches to three-dimensional applications. Concerning nonlinear problems, it should be pointed out that they can usually be linearized and solved iteratively.

Other, more specialized methods, like Fourier and cyclic reduction methods, multigrid methods or complex mapping techniques are not discussed here. See references for further reading.

4.1 Classification of partial differential equations

The general form of a second-order partial differential equation involving two independent (spatial or temporal) variables may be stated as

$$A \frac{\partial^2 \psi}{\partial x^2} + B \frac{\partial^2 \psi}{\partial x \partial y} + C \frac{\partial^2 \psi}{\partial y^2} + D \frac{\partial \psi}{\partial x} + E \frac{\partial \psi}{\partial y} + F \psi + G = 0, \quad (34)$$

where ψ is the dependent variable and x and y are the independent variables. If the coefficients A to G are functions of x and y only, the equation is said to be linear. In nonlinear equations

they also depend on ψ or its derivatives. The values of these coefficients determine the type of equation, and hence the method of solution. The important parameter is

$$\lambda = B^2 - 4AC, \quad (35)$$

and equation (34) is said to be elliptical, parabolic or hyperbolic according to whether λ is negative, zero or positive. While it is possible for the type of an equation to change within the solution domain if A , B or C vary, in the majority of practical problems this does not happen. Similar classifications can be applied to higher-order equations and to those involving more than two independent variables.

Elliptic equations normally occur in equilibrium problems, whereas the parabolic and hyperbolic types occur in propagation problems. A distinction between equilibrium and propagation problems can be made in terms of the type of conditions applied at the boundaries: The domain for an equilibrium problem is closed and boundary conditions are prescribed around the entire boundary; such a problem is often said to be of the boundary-value type. For propagation problems, one variable is the “time”, and initial values of the field have to be given for the time when the process starts. During evolution, an appropriate number of boundary conditions has to be prescribed at the boundaries of the “spatial” domain.

Obviously, the following correspondences exist between elastic problems and simpler scalar equations:

- Static elasticity and the Laplace equation (elliptical equation):

$$\frac{\partial \sigma_{ij}}{\partial x_j} = 0 \longleftrightarrow \nabla^2 \phi = 0, \quad (36)$$

- Overdamped elasticity and the diffusion equation (parabolic equation):

$$D \frac{\partial \sigma_{ij}}{\partial x_j} = \frac{\partial u_i}{\partial t} \longleftrightarrow D \nabla^2 \phi = \frac{\partial \phi}{\partial t}, \quad (37)$$

- Dynamical elasticity and the wave equation (hyperbolic equation):

$$\frac{\partial \sigma_{ij}}{\partial x_j} = \rho \frac{\partial^2 u_i}{\partial t^2} \longleftrightarrow \nabla^2 \phi = \frac{1}{c^2} \frac{\partial^2 \phi}{\partial t^2}. \quad (38)$$

In these equations, D is a kinetic coefficient and c the sound speed. Notice that the stress is basically the spatial derivative of the displacement, and therefore the expression $\partial_j \sigma_{ij}$ is a second order derivative of the displacements.

4.2 Finite difference methods

The probably simplest method to solve elastic problems is the finite difference methods. It directly discretizes the differential equations and is therefore easy to program. However, it becomes immediately much more complicated if nonuniform numerical grids are used, and then finite element methods are usually more flexible. On the other hand, finite difference methods can easily be parallelized.

Let us consider the static elastic equation, $\partial\sigma_{ij}/\partial x_j = 0$ first. As we know it describes a boundary value problem. A simple method to solve it is the *relaxation method*, i. e. we replace it by the equation

$$\frac{\partial u_i}{\partial t} = D \frac{\partial \sigma_{ij}}{\partial x_j}, \quad (39)$$

which is purely dissipative. Here, $D > 0$ is a kinetic coefficient. Notice that we introduced some artificial time dependence $u_i(t)$ in this equation, and the desired solution is obtained in the limit $t \rightarrow \infty$, since $\dot{u}_i = 0$ then. This technique is in particular very important for nonlinear problems (like in nonlinear elasticity or plasticity), but we discuss it here for simplicity only for linear problems. The analogue is the diffusion equation,

$$\frac{\partial \phi}{\partial t} = D \nabla^2 \phi, \quad (40)$$

which we can immediately identify as a parabolic equation. For the sake of brevity, we study this equation in one spatial dimension. The discrete Laplace operator becomes then

$$\nabla^2 \phi \rightarrow \frac{\phi_{j+1}^{(n)} - 2\phi_j^{(n)} + \phi_{j-1}^{(n)}}{(\Delta x)^2}. \quad (41)$$

Here, the upper index denotes the discrete time, $t = n\Delta t$, and the lower index the spatial coordinate, $x = j\Delta x$ (Δt and Δx are timestep and spatial resolution respectively). The simplest representation of the left hand side is

$$\frac{\partial \phi}{\partial t} \rightarrow \frac{\phi_j^{(n+1)} - \phi_j^{(n)}}{\Delta t}, \quad (42)$$

and thus the discrete version of the diffusion equation becomes

$$\frac{\phi_j^{(n+1)} - \phi_j^{(n)}}{\Delta t} = D \left(\frac{\phi_{j+1}^{(n)} - 2\phi_j^{(n)} + \phi_{j-1}^{(n)}}{(\Delta x)^2} \right). \quad (43)$$

This is a so called *explicit representation* of the equation, because the values $\phi_j^{(n+1)}$ at the “new” time $n+1$ can be directly expressed in terms of field values at the previous timestep. Therefore, the strategy to calculate the time evolution is very simple:

1. Initialize the field $\phi_j^{(n=0)}$ at all lattice sites to the initial values.
2. Perform a time step by explicit computation of the new values at time $n+1$ from the previous values at timestep n . Do this for all interior points.
3. Apply the boundary conditions. For Dirichlet conditions (prescribed field value $\phi = \bar{\phi}$; the overline denotes the given value), one can directly set the field values to the desired values, for von Neumann conditions (prescribed normal derivative $\partial\phi/\partial n = \overline{\partial\phi/\partial n}$), the value at the boundary has to be related to the values at the neighboring points.
4. Go back to step 2.

If only the asymptotic values are relevant, at least for linear problems the initialization in step 1 is not crucial. Since the diffusion equation is purely dissipative, the energy of the system is diminished in each timestep, and therefore one approaches the global minimum of the energy. In nonlinear problems the energy landscape is usually complicated and has many local minima from which the solution cannot escape; thus, a good guess for the equilibrium field ϕ has to be set in the initialization or more sophisticated optimization methods have to be used (e. g. Simulated Annealing).

For an *implicit method* we write

$$\frac{\phi_j^{(n+1)} - \phi_j^{(n)}}{\Delta t} = D \left(\frac{\phi_{j+1}^{(n+1)} - 2\phi_j^{(n+1)} + \phi_{j-1}^{(n+1)}}{(\Delta x)^2} \right). \quad (44)$$

Notice that on the right hand side the Laplacian is evaluated at the new time $n + 1$. Here, we can not immediately express the value $\phi_j^{(n+1)}$ through the previous values $\phi_j^{(n)}$; instead, a linear system of equations has to be solved. Fortunately, this is a simple problem because the system is tridiagonal. However, in more than one spatial dimension the system immediately becomes more complicated, because each grid points interacts with its horizontal and vertical neighbors. Then the *alternating direction implicit method* which treats the different directions separately, or more generally *operator splitting techniques*, become useful [11].

A central point in the numerical treatment of partial differential equations is stability. Obviously, the diffusion equation (40) is stable, because all modes $\phi(x, t) = \exp(\lambda t + ikx)$ decay, $\lambda = -Dk^2$. On the other hand, we can perform a *von Neumann stability analysis* of the explicit representation (43) with the ansatz $\phi_j^{(n)} = \xi^n \exp(ikj\Delta x)$. This leads to

$$\xi = 1 + \frac{2D\Delta t}{(\Delta x)^2} (\cos(k\Delta x) - 1). \quad (45)$$

For stability, we have to demand $|\xi| < 1$, because otherwise the solution grows indefinitely. This limits the maximum allowed timestep,

$$\Delta t < \frac{(\Delta x)^2}{2D}, \quad (46)$$

which becomes small for fine grids and makes the computations very inefficient.

The advantage of the more complicated implicit method is that it is unconditionally stable, because $|\xi| < 1$ for any stepsize Δt .

The wave equation $\ddot{\phi} = c^2 \nabla^2 \phi$ (c is the sound speed), in analogy to the elastodynamic equation $\partial_j \sigma_{ij} = \rho \ddot{u}_i$, can be easily discretized in an explicit scheme. For one spatial dimension, it becomes

$$\frac{\phi_j^{(n+1)} - 2\phi_j^{(n)} + \phi_j^{(n-1)}}{(\Delta t)^2} = c^2 \frac{\phi_{j+1}^{(n)} - 2\phi_j^{(n)} + \phi_{j-1}^{(n)}}{(\Delta x)^2}. \quad (47)$$

Notice that this scheme is symmetric both in space and time. It can easily be checked that the scheme is stable if $c\Delta t/\Delta x < 1$.

For elastic problems, one can conveniently use a *staggered grid*, which means that the displacements are defined on grids that are shifted by half a lattice unit. Similar gimmicks are used in hydrodynamics, but they are beyond the scope of this article.

Also, elastic simulations can be coupled to phase field simulations to describe processes with propagating interfaces like in fracture. In Fig. 7 crack growth in the unstable regime for high driving forces is shown, exhibiting successive tip splitting. See [12, 13] for details.

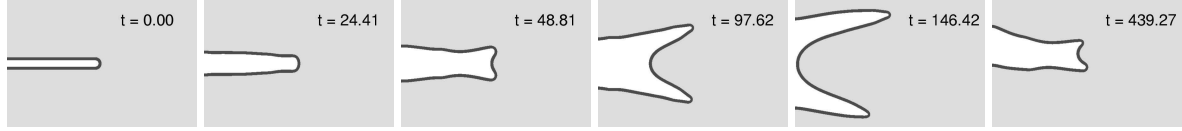


Fig. 7: Phase field modeling of an irregular crack tip splitting scenario in a strip which is pulled in vertical direction. After symmetrical growth of the sidebranches, one finger wins the competition, moves back to the center of the strip and can finally split again [13].

4.3 Finite Element Method (FEM)

A very important technique to solve elastic problems is the finite element method, which is in particular often used in engineering applications. Similarly to the finite difference method, it discretizes the whole computational domain, but it is easier to use with nonuniform grids. The central discrepancy between the two methods is that FEM reformulates the original partial differential equations as a variational problem [14].

The general variational approach to the solution of a continuum mechanics problem is to seek a stationary value for a functional U . When such a principle is used in a finite element analysis, the variation of U is carried out with respect to the values of the unknowns at the so called “nodes” of the “mesh”, a discretization of the domain. Sometimes the relevant functional can be immediately obtained from familiar physical principles. For example, the solutions to structural and elastic continuum problems can be obtained by minimizing the total potential energy, as will be seen below.

For simplicity, we illustrate the finite element method for the Laplace equation first. Again, in the domain Ω we have to solve the bulk equation $\nabla^2 \phi = 0$. We define an integral measure for the quality of solution of the Laplace equation by multiplying it with a *test function* ψ and integrate it over the domain,

$$\int_{\Omega} \psi \nabla^2 \phi d\Omega = 0.$$

Application of the product rule and Gauss’ theorem then leads to

$$\begin{aligned} 0 &= \int_{\Omega} \nabla \cdot (\psi \nabla \phi) d\Omega - \int_{\Omega} (\nabla \psi) \cdot (\nabla \phi) d\Omega \\ &= \int_{\Gamma} \psi \frac{\partial \phi}{\partial n} d\Omega - \int_{\Omega} (\nabla \psi) \cdot (\nabla \phi) d\Omega, \end{aligned} \quad (48)$$

where n is the outward pointing normal and $\Gamma = \partial\Omega$ the boundary of the domain. This relation must be satisfied for arbitrary test functions ψ if ϕ fulfills the Laplace equation. The boundary Γ is now assumed to consist of two parts, $\Gamma = \Gamma_1 + \Gamma_2$. On Γ_1 the function value $\phi = \bar{\phi}$ is prescribed, and on Γ_2 , we have von Neumann conditions, $\partial\phi/\partial n = \bar{\partial\phi/\partial n}$. Other types of boundary conditions are also possible and can be handled similarly.

For a discretization procedure, the function ϕ is assumed to depend on a set of adjustable parameters. In particular, the function values $\phi(\mathbf{r}_i)$ at certain *nodal points* \mathbf{r}_i are a possible choice for these unknowns; between these points, the function is interpolated in some way. Let a be a typical such parameter. Then we can use $\psi = \partial\phi/\partial a$ as a special case in the integral condition (48) above. Since on Γ_1 the function value is given explicitly, it cannot depend on any

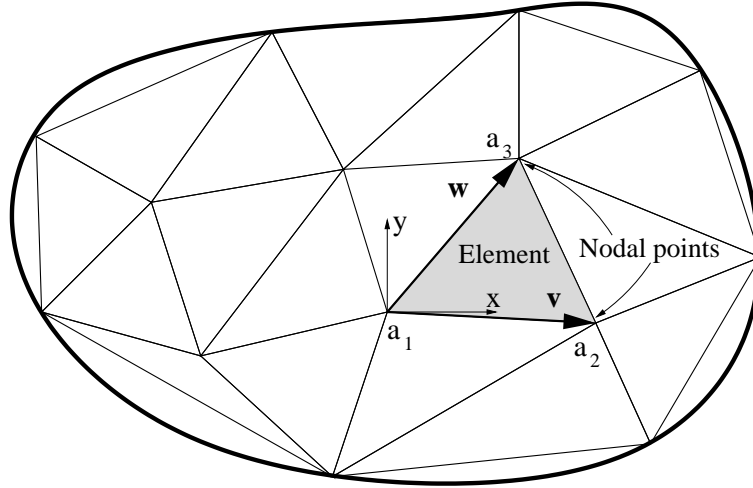


Fig. 8: Tessellation of the two-dimensional domain by triangles. Each triangle is spanned by vectors \mathbf{v} and \mathbf{w} , and a local coordinate system is introduced.

adjustable parameter, thus $\partial\phi/\partial a = 0$ there. Therefore, the above condition can be rewritten as

$$\frac{\partial U}{\partial a} = 0 \quad (49)$$

with a functional

$$U = \int_{\Omega} \frac{1}{2} (\nabla \phi)^2 d\Omega - \int_{\Gamma_2} \phi \frac{\partial \phi}{\partial n} d\Gamma. \quad (50)$$

This expression can be interpreted as the energy of the system which has to become stationary: The first term represents the bulk energy, the second is the work of the external forces. The optimization of this functional is called the *weak formulation* of the Laplace equation, since the function ϕ is differentiated only once and not twice as in the original formulation.

For example, a particular mathematical function of position involving a finite number of undetermined parameters, such as polynomials with undetermined coefficients, might be assumed for ϕ . The best fit of this approximation to the true distribution could be obtained by making the value of U stationary with respect to the function parameters. Finite element methods can be regarded as being of this type. Instead of using a single and necessarily complicated function to cover the whole solution domain, a series of relatively simple functions applicable to small subregions is employed, as will be seen below. The overall distribution of ϕ is hereby defined in terms of values at points of interconnection between the subregions. The required solution is obtained when the value of U is stationary with respect to each and every one of these point values.

Meshes of triangular elements can be devised to suit a very wide range of practical (two-dimensional) problems. The first requirement of such a mesh is that it should fit the shape of the boundary of the solution domain as closely as possible. This requirement can be met provided the boundary shape can be approximated with sufficient accuracy by a series of short straight lines which form sides of elements. Clearly, the sizes of the elements should be reduced in regions close to sharply curved boundaries. Following the same principle within the solution domain, it is desirable to have a concentration of relatively small elements in regions of the

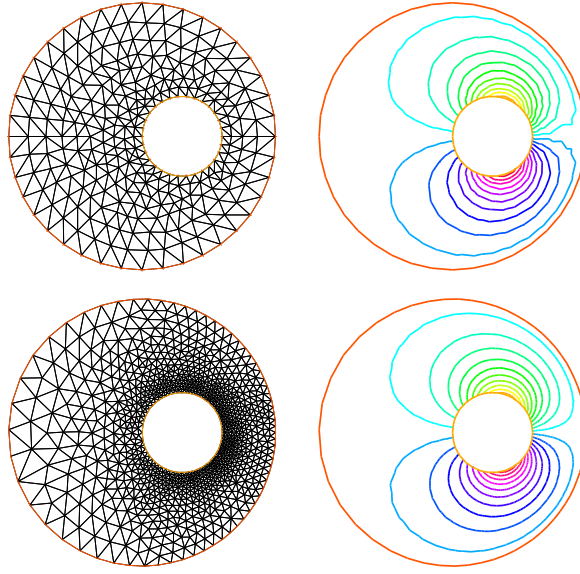


Fig. 9: Example for FEM calculations: The Laplace equation is solved in a circle with a hole. On the outer boundary, the Dirichlet condition $\phi = 1$ is applied, on the inner circle the boundary condition is $\partial\phi/\partial n = -xy$. Top row: original mesh and lines of constant potential of the first approximative solution using linear shape functions. Bottom row: The same after a mesh refinement.

domain where the unknowns are likely to change rapidly, particularly since these regions are often of greatest interest in the solution.

In the simplest case, we take the function values at the corners of the triangular *elements* as unknowns, usually referred to as *nodal points*, and assume the function ϕ to be piecewise linear inside each element

$$\phi(x, y) = C_1 + C_2x + C_3y. \quad (51)$$

Notice that the coefficients are of course different in each element and are determined by the nodal values. Therefore, the total function $\phi(x, y)$ is continuous, since the nodal values are the same in adjacent triangles; however, $\phi(x, y)$ is not smooth across the interfaces. If we denote the nodal values by a_i as in Fig. 8, the constants C_i are explicitly given by

$$\begin{aligned} C_1 &= a_1, \\ C_2 &= \frac{a_1(w_y - v_y) + a_3v_y - a_2w_y}{2\Delta}, \\ C_3 &= -\frac{a_1(w_x - v_x) + a_3v_x - a_2w_x}{2\Delta}, \end{aligned}$$

with the x and y components v_x, v_y, w_x, w_y of the vectors \mathbf{v}, \mathbf{w} respectively and the (oriented) triangle area $\Delta = (w_xv_y - v_xw_y)/2$. Notice that the local origin is in corner 1.

For illustrative purposes, we assume that we have only Dirichlet boundary conditions, hence the second integral in (50) vanishes. Inserting expression (51) into the functional (50) gives therefore

$$U = \sum_m |\Delta^{(m)}| \frac{1}{2} \left(C_2^{(m)^2} + C_3^{(m)^2} \right). \quad (52)$$

Here, summation is done on all elements m . Since the coefficients $C_i^{(m)}$ are linear functions of the unknowns a_i – the values at the nodal points –, the minimization conditions,

$$\frac{\partial U}{\partial a_i} = 0, \quad (53)$$

for all nodal points lead to a set of coupled linear equations for the unknowns a_i .

For solution of the linear problem, standard algorithms like the Gaussian elimination or the Gauss-Seidel-Method can be used. Notice that for proper arrangement of the equations the nonzero coefficients of the matrix are confined to a relatively narrow band parallel to the diagonal of the matrix. The Gaussian elimination is very robust and usually faster than the Gauss-Seidel method, but requires more memory for storage of the data. If the number of elements is rather small or the matrix not diagonally dominant, the Gaussian elimination is a good choice. The variational formulation provides general statements about the conditions for convergence of finite element methods. If the functional whose stationary value is sought involves derivatives of the unknown function up to the n th order, the shape functions employed within the elements should ensure continuity across element interfaces of derivatives up to the $(n - 1)$ th order. Elements and their associated shape functions which satisfy this requirement are said to be *conforming* or *compatible*.

Many commercial and free FEM packages exist. For illustration purposes, we use here the public domain program FreeFem++ [15]. A simple example is the following:

```
// *** FreeFem++ program ***
// definition of the mesh
border a(t=0,2*pi){x=cos(t); y=sin(t); label=1;}
border b(t=0,2*pi){x=0.3+0.3*cos(t); y=0.3*sin(t); label=2;}
mesh MyMesh = buildmesh (a(40)+b(-30));
plot(MyMesh, wait=1);

// use linear elements (P1)
fespace Vh(MyMesh,P1);
Vh phi,psi;

// define the problem
func f=-x*y;
problem laplace(phi,psi) = int2d(MyMesh)(dx(phi)*dx(psi) + dy(phi)*dy(psi))
- int1d(MyMesh,2)(f*psi) + on(1,phi=1);

// solve the problem
laplace;
plot(phi, wait=1);

// mesh refinement
MyMesh = adaptmesh(MyMesh, phi, err=0.005);
plot(MyMesh, wait=1);

// solve it again on the refined mesh
laplace;
plot(phi, wait=1);
// *** end of program ***
```

First, the mesh is defined, using two circles as outer (1) and inner boundary (2). They are discretized using 40 and 30 line segments respectively, and the region between them is filled with triangles using the automesh function of the program. We use linear elements (P1) as described above. Next, the problem is defined in a variational formulation. We explicitly demand Dirichlet conditions $\phi = 1$ on the outer boundary (1) and von Neumann conditions $\partial\phi/\partial n = -xy$ on the inner boundary (2) (the origin is in the center of the system). The following mesh refinement

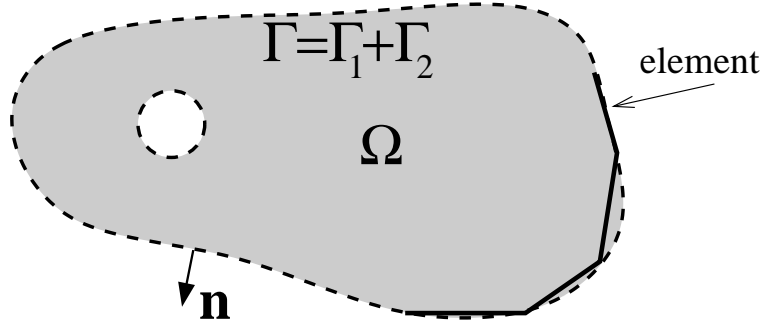


Fig. 10: The boundary integral method. On the boundary of the domain Ω either Dirichlet or von Neumann boundary conditions are prescribed. The boundary can be multiply connected. In the right corner the discretization through boundary elements is sketched.

is very useful as it adapts the mesh such that it can represent the field to a prescribed accuracy. Finally, the problem is solved again on the new mesh. The results are shown in Fig. 9.

The method can immediately be extended to elastostatic problems (we illustrate it for two dimensions here). Instead of an unknown scalar field $\phi(x, y)$ we now have two unknown functions $u_x(x, y)$ and $u_y(x, y)$ in a plane strain scenario. The proper functional is the elastic energy together with the work exerted by the external forces,

$$U = \int_{\Omega} \frac{1}{2} \sigma_{ik} \epsilon_{ik} d\Omega - \int_{\Gamma_2} \bar{\sigma}_{in} u_i d\Gamma, \quad (54)$$

where we assume that fixed displacements are prescribed on the interface contour Γ_1 and tractions $\bar{\sigma}_{in}$ are given on Γ_2 . We can use linear shape functions, $u_x = C_1 + C_2x + C_3y$ and $u_y = C_4 + C_5x + C_6y$ on each triangular element. Variation of the energy (54) with respect to the unknowns, the displacements at the corners of the triangles, leads again to a set of linear equations.

4.4 Boundary Element Method (BEM)

The boundary element method (or boundary integral method) differs from the two previous techniques in the sense that only a discretization of the boundary surrounding the domain is required. For simplicity, we look at the Laplace equation first. In the domain Ω the bulk equation $\nabla^2 \phi = 0$ has to be fulfilled. As before, we consider two types of boundary conditions here; we therefore assume the total boundary Γ to consist of two parts Γ_1 and Γ_2 . *Dirichlet conditions* on Γ_1 mean that the function value is prescribed there, $\phi = \bar{\phi}$ (the bar denotes known values); *Von Neumann conditions* on Γ_2 correspond to given normal derivatives of the function, $\partial\phi/\partial n = \bar{\partial\phi/\partial n}$. The normal vector is oriented outward the domain Ω (see Fig. 10). It is allowed to have disconnected boundaries, i. e. holes in the domain Ω .

The basic idea of the boundary integral method is to use the known Green function for an infinite system. For the case of the two-dimensional Laplace equation it is given by

$$\phi^*(\mathbf{r}, \mathbf{r}_0) = \frac{1}{2\pi} \ln \frac{1}{|\mathbf{r} - \mathbf{r}_0|} \quad (55)$$

and obeys the equation

$$\nabla^2 \phi^* = -\delta(\mathbf{r} - \mathbf{r}_0) \quad (56)$$

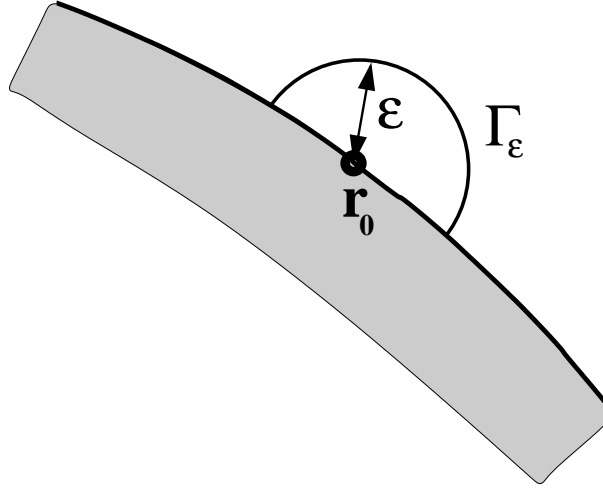


Fig. 11: The boundary is augmented by a semicircle in case of a boundary point.

with the Dirac delta distribution δ .

According to the Laplace equation, we have for any point \mathbf{r}_0 inside Ω (not on the boundary)

$$\int_{\Omega} \phi^*(\mathbf{r}, \mathbf{r}_0) \nabla^2 \phi d\Omega = 0.$$

On the other hand, we can use Gauss' theorem twice and obtain

$$\begin{aligned} 0 &= \int_{\Omega} \phi^* \nabla^2 \phi d\Omega = \int_{\Omega} \nabla \cdot (\phi^* \nabla \phi) d\Omega - \int_{\Omega} (\nabla \phi^*) \cdot (\nabla \phi) d\Omega \\ &= \int_{\Gamma} \phi^* \frac{\partial \phi}{\partial n} d\Gamma - \int_{\Omega} \nabla \cdot (\phi \nabla \phi^*) d\Omega + \int_{\Omega} \phi \nabla^2 \phi^* d\Omega \\ &= \int_{\Gamma} \phi^* \frac{\partial \phi}{\partial n} d\Gamma - \int_{\Gamma} \phi \frac{\partial \phi^*}{\partial n} d\Gamma - \phi(\mathbf{r}_0), \end{aligned}$$

where in the last step we have used the property of the Green function (56). Thus the value of the field ϕ at any inner point \mathbf{r}_0 can be expressed through a boundary integral

$$\phi(\mathbf{r}_0) = \int_{\Gamma} \phi^* \frac{\partial \phi}{\partial n} d\Gamma - \int_{\Gamma} \phi \frac{\partial \phi^*}{\partial n} d\Gamma. \quad (57)$$

However, from the boundary conditions either only ϕ or $\partial \phi / \partial n$ is known.

For reasons that will become obvious soon, it makes sense to let the internal point \mathbf{r}_0 come close to the boundary, because then the values of ϕ on Γ can also be expressed through boundary integrals. A simple way to do this is to consider that the point \mathbf{r}_0 is on the boundary but the domain itself is augmented by a semicircle of radius ϵ . The point \mathbf{r}_0 is considered to be at the center and then the radius ϵ is taken to zero. For simplicity, we discuss only smooth surfaces as represented in Fig. 11; the case of corners is studied in detail in the literature. The reason for this complicated procedure is that the integrands become singular and one has to be careful when calculating them.

Let us look at the first integral in Eq. (57). It can be split into two integrals, one along the semicircle Γ_{ϵ} and the other along $\Gamma - \Gamma_{\epsilon}$. The latter one becomes in the limit $\epsilon \rightarrow 0$ a principal

value integral, and we can evaluate the other one explicitly:

$$\lim_{\epsilon \rightarrow 0} \left\{ \int_{\Gamma_\epsilon} \phi^* \frac{\partial \phi}{\partial n} d\Gamma \right\} = - \lim_{\epsilon \rightarrow 0} \left\{ \int_{\Gamma_\epsilon} \frac{1}{2\pi} \ln \epsilon \frac{\partial \phi}{\partial n} d\Gamma \right\} = - \lim_{\epsilon \rightarrow 0} \left\{ \frac{\epsilon}{2} \ln \epsilon \frac{\partial \phi}{\partial n} \right\} = 0.$$

Here we assume that the function ϕ is smooth in the vicinity of the point \mathbf{r}_0 . Similarly, for the core contribution to the second integral,

$$\lim_{\epsilon \rightarrow 0} \left\{ \int_{\Gamma_\epsilon} \phi \frac{\partial \phi^*}{\partial n} d\Gamma \right\} = - \lim_{\epsilon \rightarrow 0} \left\{ \int_{\Gamma_\epsilon} \phi \frac{1}{2\pi\epsilon} d\Gamma \right\} = - \lim_{\epsilon \rightarrow 0} \left\{ \phi \frac{\epsilon}{2\epsilon} \right\} = -\frac{1}{2} \phi(\mathbf{r}_0).$$

Consequently, for a point \mathbf{r}_0 on the boundary we have

$$\frac{1}{2} \phi(\mathbf{r}_0) = \int_{\Gamma} \phi^* \frac{\partial \phi}{\partial n} d\Gamma - \int_{\Gamma} \phi \frac{\partial \phi^*}{\partial n} d\Gamma, \quad (58)$$

where the integrals are in the sense of a Cauchy principal value. This equation is generally used as a starting point for the boundary element method.

Let us now consider how expression (58) can be discretized to find the system of equations from which the boundary values can be determined. Assume that the boundary is divided into N straight segments or *elements* as shown in Fig. 10. For the simplest case of so called *constant elements* the function values ϕ and $\partial\phi/\partial n$ are assumed to be constant along each element. The coordinates \mathbf{r}_0 on the boundary are enumerated by a discrete index $i = 1 \dots N$. They are defined in the center of the elements, also called *nodes*. Then Eq. (58) becomes

$$\frac{1}{2} \phi^{(i)} = \sum_{j=1}^N \int_{\Gamma^{(j)}} \phi \frac{\partial \phi^*}{\partial n} d\Gamma - \sum_{j=1}^N \int_{\Gamma^{(j)}} \frac{\partial \phi}{\partial n} \phi^* d\Gamma \quad (59)$$

with the straight elements $\Gamma^{(j)}$. The values ϕ and $\partial\phi/\partial n$ can be taken out of the integrals since they are constant along each (small) element. They are called $\phi^{(j)}$ and $(\partial\phi/\partial n)^{(j)}$ for element j . Remember that the the Green function and its normal derivative still depend on \mathbf{r}_0 or – in the discrete version – on the the index i . We can define *influence coefficients*

$$H^{(ij)} = \int_{\Gamma^{(j)}} \frac{\partial \phi^*}{\partial n} d\Gamma, \quad G^{(ij)} = \int_{\Gamma^{(j)}} \phi^* d\Gamma. \quad (60)$$

Since they depend only on the Green function or its derivative, these are known expressions for a given discretization. They can be computed either analytically or numerically. For the diagonal terms $i = j$ it is usually best to use analytical expressions since the kernels are singular and the integrals have to be interpreted as Cauchy principal value integrals. Due to symmetry (remember that the node is in the middle of the element), we have

$$H^{(ii)} = \int_{\Gamma^{(i)}} \frac{\partial \phi^*}{\partial n} d\Gamma = 0. \quad (61)$$

For $G^{(ii)}$ we obtain

$$G^{(ii)} = \int_{\Gamma^{(i)}} \phi^* d\Gamma = -\frac{1}{2\pi} \int_{x=-\ell^{(i)}/2}^{\ell^{(i)}/2} \ln |x| dx = \frac{\ell^{(i)}}{2\pi} [-\ln(\ell^{(i)}/2) + 1], \quad (62)$$

with $\ell^{(i)}$ being the length of the element i .

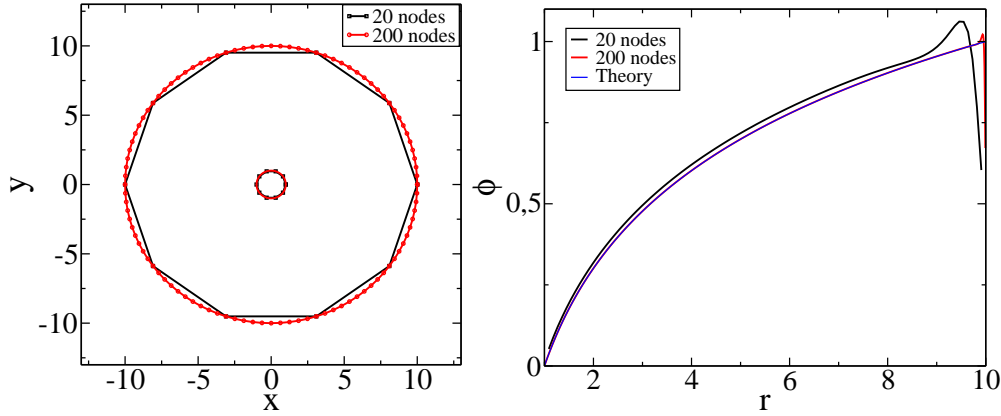


Fig. 12: Numerical solution of the two-dimensional Laplace equation using the boundary integral method in the domain defined by two concentric circles.

Hence we obtain for each interface point

$$\frac{1}{2}\phi^{(i)} + \sum_{j=1}^N H^{(ij)}\phi^{(j)} = \sum_{j=1}^N G^{(ij)} \left(\frac{\partial\phi}{\partial n} \right)^{(j)}. \quad (63)$$

By boundary conditions, either $\phi^{(i)}$ or $(\partial\phi/\partial n)^{(i)}$ is given, so we have altogether N unknowns and also N linear equations to determine these unknowns. Thus Eq. (63) can be cast into a matrix problem which can be solved using ordinary linear algebra routines. Notice that the matrices which appear here are usually not sparse. We refer to the article by I. Gutheil for solution of the linear equations.

Once the problem is solved completely, the values of ϕ and $\partial\phi/\partial n$ can be calculated not only on the boundary, but also all values can be computed inside the domain Ω using Eq. (57), since now the right hand side of this equation is known.

A illustration of the method is shown in Fig. 12. The solution of the Laplace equation $\nabla^2\phi = 0$ for two concentric circles (inner radius $R_i = 1$, outer radius $R_o = 10$) with prescribed potentials $\phi_i = 0$ and $\phi_o = 1$ is $\phi(r) = \log r / \log R_o$. Two numerical discretizations of the (disconnected) boundaries are used, and obviously the solution agrees very well with the analytical solution at least in the region not too close to the boundaries.

For elasticity, the procedure is similar. We consider only static elasticity and neglect all body forces; the method can easily be extended to account for these “force terms”. The elastic equation is

$$\frac{\partial\sigma_{ik}}{\partial x_k} = 0 \quad (64)$$

in the bulk, and boundary conditions are either for displacements ($u_i = \bar{u}_i$ on Γ_1), corresponding to Dirichlet conditions, or for stresses ($\sigma_{nj} = \sigma_{ij}n_i = \bar{\sigma}_{nj}$ on Γ_2), similar to the von Neumann conditions in the potential problem. For a two-dimensional situation, at each interface point two boundary conditions have to be prescribed.

By u_k^{l*} we denote the Green function of the infinite medium for a point force in \mathbf{r}_0 (as before, we do not write the location of the source \mathbf{r}_0). The force is acting in the l direction, and the Green function gives the k component of the resulting displacement everywhere in the medium. From this expression we can also derive the resulting strain, $\epsilon_{ik}^{l*} = (\partial_i u_k^{l*} + \partial_k u_i^{l*})/2$, and, with

the help of Hooke's law, the stresses σ_{ik}^{l*} . By definition, they fulfill the equation

$$\frac{\partial \sigma_{ik}^{l*}}{\partial x_k} = -\delta(\mathbf{r} - \mathbf{r}_0)\delta_{il}. \quad (65)$$

The Green function for an isotropic material in plane strain is

$$u_k^{l*} = \frac{1}{8\pi\mu(1-\nu)} \left[-(3-4\nu)\ln(r)\delta_{lk} + \frac{\partial r}{\partial x_l} \frac{\partial r}{\partial x_k} \right] \quad (66)$$

which gives the response of the displacement in k direction at a distance $r = x_i^2$ from the point source to a unit force in l direction located at the origin; $\mu = E/[2(1+\nu)]$ is the shear modulus. Now we perform the integration by parts twice as before:

$$\begin{aligned} 0 &= \int_{\Omega} \frac{\partial \sigma_{ik}}{\partial x_k} u_i^{l*} d\Omega = \int_{\Omega} \frac{\partial}{\partial x_k} (\sigma_{ik} u_i^{l*}) d\Omega - \int_{\Omega} \sigma_{ik} \epsilon_{ik}^{l*} d\Omega \\ &= \int_{\Gamma} \sigma_{in} u_i^{l*} d\Gamma - \int_{\Omega} \epsilon_{ik} \sigma_{ik}^{l*} d\Omega \\ &= \int_{\Gamma} \sigma_{in} u_i^{l*} d\Gamma - \int_{\Omega} \frac{\partial}{\partial x_k} (u_i \sigma_{ik}^{l*}) d\Omega + \int_{\Omega} u_i \frac{\partial \sigma_{ik}^{l*}}{\partial x_k} d\Omega \\ &= \int_{\Gamma} \sigma_{in} u_i^{l*} d\Gamma - \int_{\Gamma} u_i \sigma_{in}^{l*} d\Gamma - u_l(\mathbf{r}_0). \end{aligned} \quad (67)$$

In the first step we used the bulk equation (64) and the symmetry of the stress and strain tensor. In the second step we used the self-adjointness of the ‘‘Hooke’’ operator, i. e. the property that $\sigma_{ik} \epsilon_{ik}^{l*} = \epsilon_{ik} \sigma_{ik}^{l*}$ (the straightforward way to see this is to write down the full expression explicitly). Eq. (65) was used in the last step. In the limiting case that the point \mathbf{r}_0 is on the boundary, the latter equation becomes

$$\frac{1}{2} u_l(\mathbf{r}_0) = \int_{\Gamma} \sigma_{in} u_i^{l*} d\Gamma - \int_{\Gamma} u_i \sigma_{in}^{l*} d\Gamma, \quad (68)$$

similarly to Eq. (58). Again the integrals now have to be interpreted in the sense of a Cauchy principal value. The discretization procedure is the same as above and carefully explained in [16, 17].

4.5 Discussion

All the presented methods are extensively used in practical applications, and of course many refinements exists to improve the general ideas shown here.

The main advantage of the finite difference methods is that they are (at least for explicit schemes) very easy to program on regular grids. Also, they can be parallelized in a simple way. The main disadvantage of the explicit schemes is that the maximum allowed timestep dramatically diminishes for finer and finer grids. Implicit methods, which require the solution of linear problems at each timestep, can be used to overcome this limitation.

For non-uniform meshes, the implementation of the finite difference methods becomes tedious, and finite element methods are more useful. They are mainly used in engineering applications, because many (commercial) packages exist for all kind of problems, and of course they can also be used for three-dimensional applications. Auto-meshing routines help to concentrate

more elements in regions where the fields strongly vary and therefore to optimize the efficiency of the calculations, especially when several lengthscales exist in the problem. However, the disadvantage of third-party libraries is less flexibility in adjusting the code to specific problems. Boundary integral techniques offer the great advantage that only the boundary has to be discretized. In particular, for two-dimensional problems (for which they are most suited) the boundary is only one-dimensional and can easily be traced. This is especially important for sharp interface calculations in pattern formation processes where the boundaries between different “phases” move in the course of time. Particular examples are melting and solidification processes or fracture. Notice, for comparison, that in finite element methods the grid has to be re-meshed after a few timesteps, which is highly time-consuming.

Appendices

A The static semi-infinite crack

In this section we derive the elastic fields for an infinite solid which contains a semi-infinite straight crack. In particular, we are interested in the divergent part of the stresses in the vicinity of the infinitely sharp crack tip.

We consider a two-dimensional, plane strain situation. We make a separation ansatz for the Airy function (13)

$$U = Ar^m e^{in\theta}$$

in polar coordinates ($\theta = 0$ in front of the crack; $\theta = \pm\pi$ is the crack surface), with r being the distance from the crack tip; n and m are arbitrary real numbers. Real and imaginary parts of the Airy function are intended to be independent solutions.

Since in polar coordinates

$$\Delta = \frac{\partial^2}{\partial r^2} + \frac{1}{r^2} \frac{\partial}{\partial \theta^2} + \frac{1}{r} \frac{\partial}{\partial r},$$

we obtain

$$\Delta \Delta U = A e^{in\theta} r^{m-4} (m^2 - n^2) ((m-2)^2 - n^2).$$

Thus we get 4 independent real solutions of the fourth order equation (14) with either $n = m$ or $n = m - 2$

$$\begin{aligned} U^{(1)} &= r^m \cos m\theta, & U^{(2)} &= r^m \sin m\theta, \\ U^{(3)} &= r^m \cos(m-2)\theta, & U^{(4)} &= r^m \sin(m-2)\theta. \end{aligned}$$

We study only singular stress states with $m < 2$. They exhibit the characteristic singularity of stresses at the crack tip.

The spatial derivatives are

$$\begin{aligned} \left(\frac{\partial}{\partial x} \right)_y &= \cos \theta \left(\frac{\partial}{\partial r} \right)_\theta - \frac{\sin \theta}{r} \left(\frac{\partial}{\partial \theta} \right)_r \\ \left(\frac{\partial}{\partial y} \right)_x &= \sin \theta \left(\frac{\partial}{\partial r} \right)_\theta + \frac{\cos \theta}{r} \left(\frac{\partial}{\partial \theta} \right)_r \end{aligned}$$

For *mode I loading* with an external force perpendicular to the crack plane, the fundamental solutions containing \sin are forbidden by symmetry (they correspond to shear forces). The

general solution is thus a linear combination of $U^{(1)}$ and $U^{(3)}$. They lead to stress components according to Eqs. (13)

$$\begin{aligned}
 \sigma_{xx}^{(1)} &= -r^{m-2}m(m-1)\cos(m-2)\theta \\
 \sigma_{xx}^{(2)} &= r^{m-2}\left((-m^2+3m-2)\cos(m-4)\theta+2(m-1)\cos(m-2)\theta\right) \\
 \sigma_{xy}^{(1)} &= r^{m-2}m(m-1)\sin(m-2)\theta \\
 \sigma_{xy}^{(2)} &= r^{m-2}(m^2-3m+2)\sin(m-4)\theta \\
 \sigma_{yy}^{(1)} &= r^{m-2}m(m-1)\cos(m-2)\theta \\
 \sigma_{yy}^{(2)} &= r^{m-2}\left((m^2-3m+2)\cos(m-4)\theta+2(m-1)\cos(m-2)\theta\right)
 \end{aligned}$$

where the superscript 1 corresponds to $n = m$ and 2 to $n = m - 2$.

Boundary conditions require that the normal and shear components of the total stress

$$\sigma_{ij} = A_1\sigma_{ij}^{(1)} + A_2\sigma_{ij}^{(2)}$$

vanish on the cut $x < 0, y = 0$ or $\theta = \pm\pi$ for properly chosen weight factors A_1 and A_2 . The determinant solvability condition

$$\det \begin{pmatrix} \sigma_{yy}^{(1)}(\theta = \pm\pi) & \sigma_{yy}^{(2)}(\theta = \pm\pi) \\ \sigma_{xy}^{(1)}(\theta = \pm\pi) & \sigma_{xy}^{(2)}(\theta = \pm\pi) \end{pmatrix} = 0$$

leads to the equation

$$-r^{2m-4}m\sin(2m\pi)(m-1)^2 = 0.$$

Possible solutions are

$$m = 0, \quad m = 1, \quad m = 0, \pm\frac{1}{2}, \pm 1, \pm\frac{3}{2}, \pm 2, \dots$$

We are currently interested in solutions with finite energy in the tip region, i.e. $\sigma^2 r < \infty$ for $r \rightarrow 0$. Consequently, we demand $m \geq 3/2$. On the other hand, we search for singular contributions with $\sigma \rightarrow \infty$ for $r \rightarrow 0$, which imposes $m < 2$. Thus only $m = 3/2$ remains; it leads to the well-known $r^{1/2}$ -singularity of the stresses. The solution is $A_1 = A_2/3 = K_I/(2\pi)^{1/2}$, where we introduced the mode I stress intensity factor K_I . We finally obtain

$$\begin{pmatrix} \sigma_{xx} \\ \sigma_{xy} \\ \sigma_{yy} \end{pmatrix} = \frac{K_I}{(2\pi r)^{1/2}} \cos(\theta/2) \begin{pmatrix} 1 - \sin(\theta/2) \sin(3\theta/2) \\ \sin(\theta/2) \cos(3\theta/2) \\ 1 + \sin(\theta/2) \sin(3\theta/2) \end{pmatrix}. \quad (69)$$

This is the exact solution for the singular part the stress field for a semi-infinite crack. It does not contain a homogeneous contribution which arises due to the tensile force which is applied infinitely far away. For a finite crack of length L , the preceding results are valid at distances r from the tip which are much smaller than the crack length, $r \ll L$.

References

- [1] L. D. Landau and E. M. Lifshitz, *Course of Theoretical Physics, Vol. 7: Theory of Elasticity*, Butterworth-Heinmann, 1995.
- [2] N. I. Muskhelishvili, *Some Basic Problems of the Mathematical Theory of Elasticity*, Kluwer Academic Publishers, 1977.
- [3] A. A. Griffith, *The phenomena of rupture and flow in solids*, Philos. Trans. Roy. Soc. (London) A **221**, 163 (1921).
- [4] J. R. Rice, Mathematical analysis in the mechanics of fracture. In *Fracture: An Advanced Treatise*, edited by H. Liebowitz; Academic, New York, 1968.
- [5] J. Fineberg and M. Marder, *Instability in dynamic fracture*, Physics Reports **313**, 1 (1999).
- [6] B. N. J. Persson, O. Albohr, G. Heinrich, and H. Ueba, *Crack propagation in rubber-like materials*, J. Phys. Cond. Mat. **17**, R1071 (2005).
- [7] S. M. Rubinstein, G. Cohen, and J. Fineberg, *Detachment fronts and the onset of dynamic friction*, Nature **430**, 1005 (2004).
- [8] B. N. J. Persson, *Sliding Friction*, Springer, 2000.
- [9] J. P. Hirth and J. Lothe, *Theory of Dislocations*, Wiley, 1982.
- [10] D. Turcotte and G. Schubert, *Geodynamics*, Cambridge University Press, 2002.
- [11] W. H. Press et al., *Numerical Recipes in C*, Cambridge University Press, 1993 (also available for other programming languages).
- [12] K. Kassner et al., *Phase-field modeling of stress-induced instabilities*, Phys. Rev. E **63**, 036117 (2001).
- [13] R. Spatschek et al., *Phase Field Modeling of Fast Crack Propagation*, Phys. Rev. Lett. **96**, 015502 (2006).
- [14] R. T. Fenner, *Finite Element Methods for Engineers*, Imperial College Press, 1996.
- [15] <http://www.freefem.org>.
- [16] C. A. Brebbia and J. Dominguez, *Boundary Elements, An Introductory Course*, McGraw-Hill, 1989.
- [17] *Computational Methods in Contact Mechanics*, edited by M. H. Aliabadi and C. A. Brebbia, Elsevier Applied Science, 1993.